Available online at www.sciencedirect.com
SCIENCE DIRECT®
Journal of Sound and Vibration 271 (2004) 411–439
JOURNAL OF SOUND AND VIBRATION
www.elsevier.com/locate/jsvi

Hydrodynamic shock of elastic structures impacting on the water: theory and experiments

A. Carcaterra[a,*], E. Ciappi[b]

[a] *Department of Mechanics and Aeronautics, University 'La Sapienza', Via Eudossiana 18, Rome 00184, Italy*
[b] *INSEAN Italian Ship Model Basin, Rome, Italy*

Received 23 April 2002; accepted 12 February 2003

Abstract

The aim of this paper is to provide a theoretical and experimental analysis of the response of an elastic system carried on board a wedge-shaped body impacting the water surface. The wedge entering the water has a sudden deceleration with shock characteristics, resulting in a short-time duration and a sharp peak value. On the other hand, the carried system undergoes an oscillatory motion induced by the inertial load generated by the impact. The study of this problem reveals the occurrence of special conditions in the response of the on-board oscillator, depending on the parameters associated with the water entry problem, that lead to large elastic forces. The experiments show that when varying the characteristic natural frequency of the on-board oscillator, critical impact conditions occur characterized by very large amplitudes of the structural response that confirm the theoretical predictions. The analysis, based on the water shock spectral response developed by the authors in some previous papers, is generalized here and validated experimentally.

1. Introduction

The scientific interest in the entry of a rigid body into water originated in the 1930s with the pioneer works of Von Karman [1] and Wagner [2], while the technical interest was initially connected with hydrodynamic loads on seaplane floats. Twenty years later the attention was addressed to ship design, especially when considering the hydrodynamic loads on the flat bottoms of large ships, such as oil tankers [3]. During the seventies the water entry problem began to account for the elasticity of the plunging structure following the general statements of the theory

*Corresponding author. Tel.: 39-06-445-85-794; fax: 39-06-484-854.
E-mail address: a.carcaterra@dma.ing.uniroma1.it (A. Carcaterra).

0022-460X/$ - see front matter
doi:10.1016/j.jsv.2003.02.005

of hydro-elasticity given in the fundamental work by Bishop and Price [4]. More recently, a renewed interest in this field was led by the design of fast ships where light structures impact at high speed and on the rough sea [5,6] with in addition a high frequency of impacts emphasizing the fatigue damage to the materials.

The phenomenon of a structure impacting on the water surface implies, in general, very large forces, being a considerable mass of water displaced in a very short time. For purpose of illustration, in Figs. 1(a–d) and 2(a–d) an impact photograph sequence of a test model is shown from two different perspectives.

Most of the efforts addressed to the analysis of the slamming phenomena deal with the entry of rigid bodies into water. Besides the analytical solutions available for two and three dimensional simplified geometries, based on the Wagner linearized formulation [7,8], several analytical–numerical models have been developed for two-dimensional and axisymmetric bodies [9–11]. However, it is well known that, for high-speed marine vehicles characterized by very light materials, the global and local dynamic response of the structure to impact loads is an important item to consider. In fact, in this case, the hydroelastic interaction introduces additional difficulties and increases the computational time considerably when solving the coupled problem numerically. Therefore classical formulations based on the finite element analysis of the structure and boundary element method analysis of the fluid domain [12,13] allow very accurate solutions for a given set of initial conditions but are unsuitable to perform parametric analysis. On the other hand, existing experimental works, performed to evaluate the hydrodynamic force or the hydrodynamic pressure and the stress in beams and plates [6], are mainly devoted to the validation of numerical codes and to the reproduction of only particular impact conditions. Moreover, in these cases the system presents a complexity that does not allow the formulation of simple rules

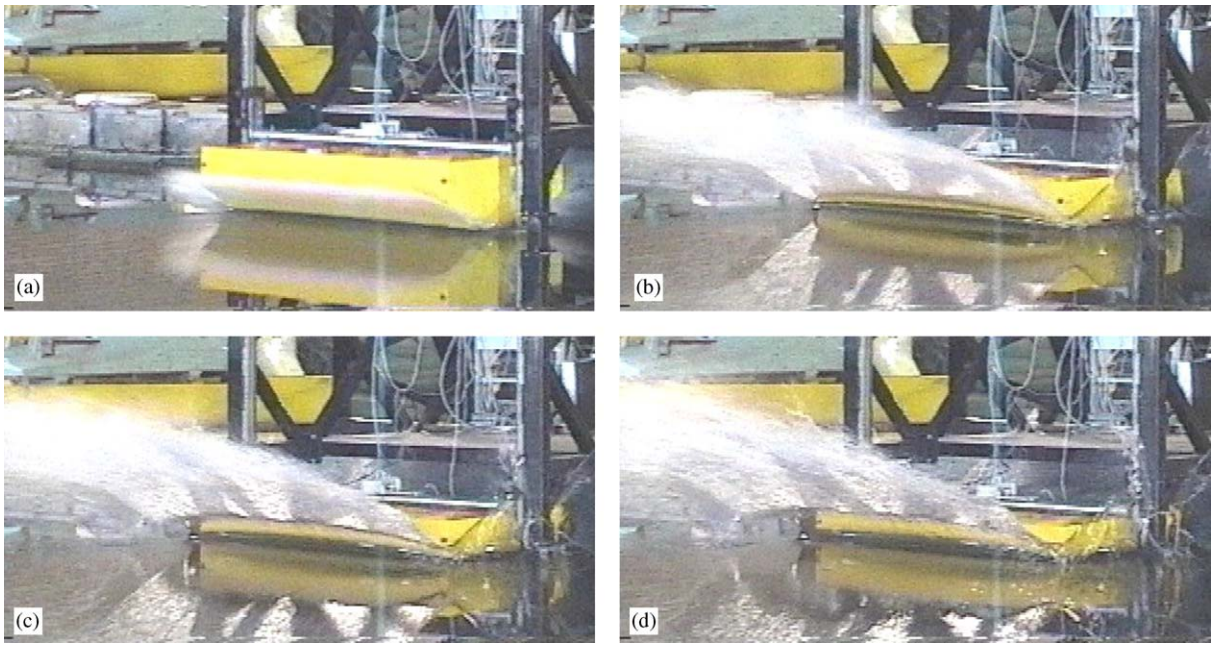

Fig. 1. (a) (b) (c) (d) Photograph sequence of the falling wedge (side view).

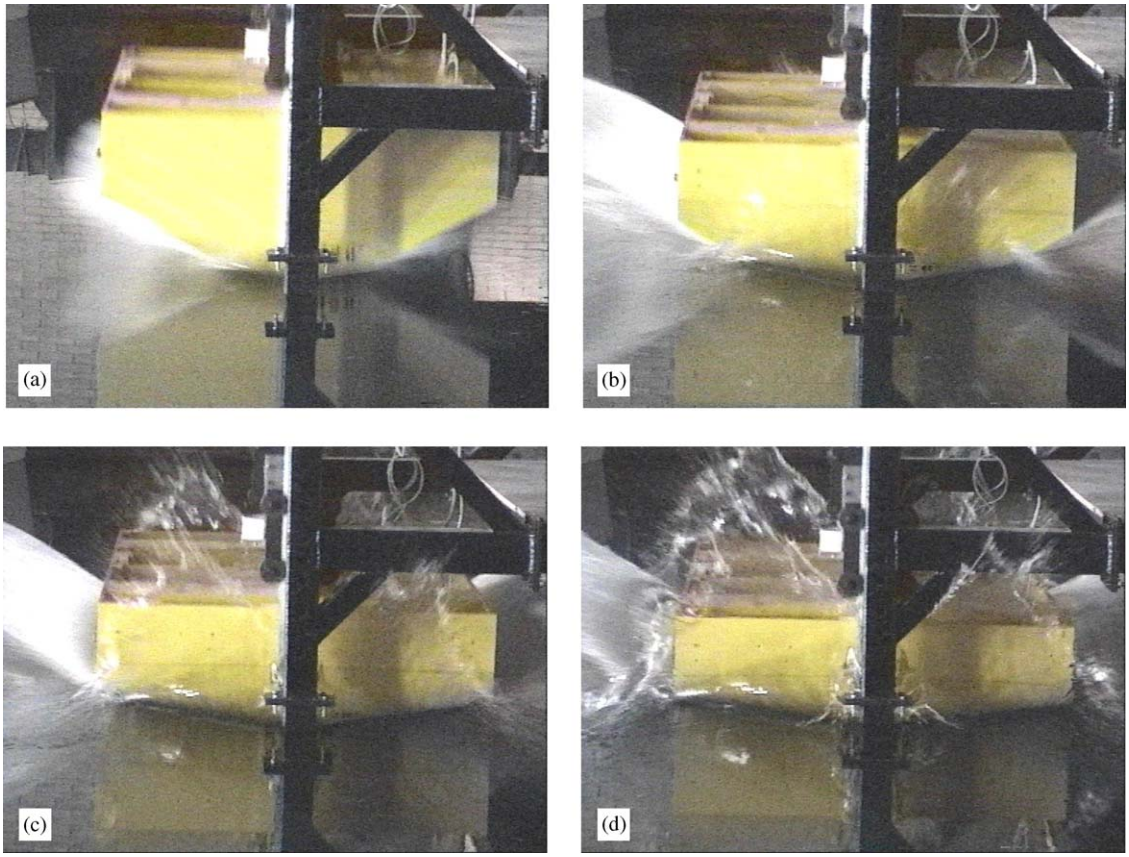

Fig. 2. (a) (b) (c) (d) Photograph sequence of the falling wedge (front view).

predicting how the hydroelastic response is affected by modifying the basic impact parameters (such as the initial impact velocity, the mass of the plunging body, etc.).

A first attempt to provide a parametric analysis of the coupled hydroelastic problem is presented in Ref. [14] where a model consisting of a rigid impacting body carrying a sprung mass is considered. The hydrodynamic model used there is that given in Ref. [10], implying a geometrical linearization of the problem (at the water-body interface) but fully considering the hydrodynamic non-linearity (quadratic velocity contributions retained in the Bernoulli equation, while they are absent in the Wagner formulation). In Ref. [14] an experimental set up for rigid-body impact is also described and the results successfully compared with the theoretical ones. On the basis of the introduced hydrodynamic model, numerical simulations of the response of the two-mass model are performed leading to interesting statements concerning the influence of the system parameters on the hydrodynamic force (or body acceleration) and sprung mass induced motion.

More recently in Refs. [15,16] a similar system has been investigated providing a good understanding of the influence of the fluid and structural parameters involved in the phenomenon, leading to closed-form relationships for the maximum force (or acceleration) of the impacting body, as well as for the elastic reaction between the two masses. Such an analysis is made possible

by the introduction of the shock spectrum approach to the vibration induced by the slamming phenomenon in combination with the use of the Wagner hydrodynamic model, producing simple prediction formulas.

Analyses, such as those in Ref. [14] or Refs. [15,16], have practical implications on the engineering ground when new devices for slamming effect attenuation have to be conceived as shown in Refs. [17,18].

In the present work, a generalization of the theoretical approach developed in Refs. [15,16], based on the use of the shock spectrum theory aimed to identify critical phenomena, is presented, and a new type of experimental set up is designed, where besides a rigid impacting body an elastic structure is fitted on board. The results of the experiments, shown in Section 4, show that critical impact conditions exist and the theoretical analysis explains why and how these critical effects are observed in practice.

Consider a rigid-body impacting the water surface with a given initial velocity. The hydrodynamic force exhibits a characteristic time history. On one hand, the drop velocity decay causes a reduction of the slamming pressure but, simultaneously, the wetted area increases. These two effects act in opposite directions on the hydrodynamic force which is the product of the average pressure times the wetted area. Initially, the latter effect dominates over the former and the force increases from its initial zero value. At t^* the two opposite phenomena find an equilibrium leading to a maximum hydrodynamic force F^*. Later, the velocity reduction effect definitively prevails and the hydrodynamic force is progressively reduced to zero.

As it will be clear in the following, the existence of this typical trend of the force is crucial to determine the response of the elastic system on board. In this frame it is in fact intuitive that a relevant role is played by the ratio between t^* and the natural period of the elastic oscillations.

The experimental investigation is performed on a wedge-shaped body supposed to be rigid and on an elastic system carried on board. Thus, the first set of tests is devoted to the measurement of the time history of the hydrodynamic force acting on the wedge. From these measurements the quantity F^* and t^* are determined. The second set of experiments is used to validate the shock spectrum approach.

In Section 2 an analytical model for the water entry of a wedge-shaped body is developed. This model admits an analytical solution that allows calculation, in closed form, of the expressions of F^* and t^*. This solution is used to predict the maximum acceleration of the elastic system carried on board leading to the estimate of the peaks' amplitude. In Section 3 the design of the experimental apparatus is described. The attention is addressed to an experimental set up reproducing as close as possible the conditions of the theoretical model. Finally, in Section 4 the results of the tests are shown and the comparison between the theoretical and the experimental data is discussed.

2. Theoretical modelling of the critical impact phenomenon

In this section the hydrodynamic impact force is determined on the basis of an analytical approach. The advantage of this point of view, with respect to the numerical solutions, relies on the chance of determining the hydrodynamic force in closed form. This is a crucial point when performing a parametrical study of the structural response to water impact loads.

For clarity, the analysis of the impact of a simple rigid wedge is developed in Section 2.1, while in Section 2.2 the analysis of a rigid wedge carrying a simple spring–mass system is considered, assuming the hypothesis that the elastic force is considerably lower than the hydrodynamic one and thus its contribution in evaluating the hydrodynamic load is negligible (weak hydro-elastic interaction).

2.1. Impact of the rigid wedge

Consider a two-dimensional rigid wedge (see Figs. 3(a) and (b)) of mass m per unit length, impacting on the water surface with an initial drop velocity v_0. The equation of motion simply reads

$$m\ddot{\zeta} = -F_h(\zeta, \dot{\zeta}, \ddot{\zeta}), \tag{1}$$

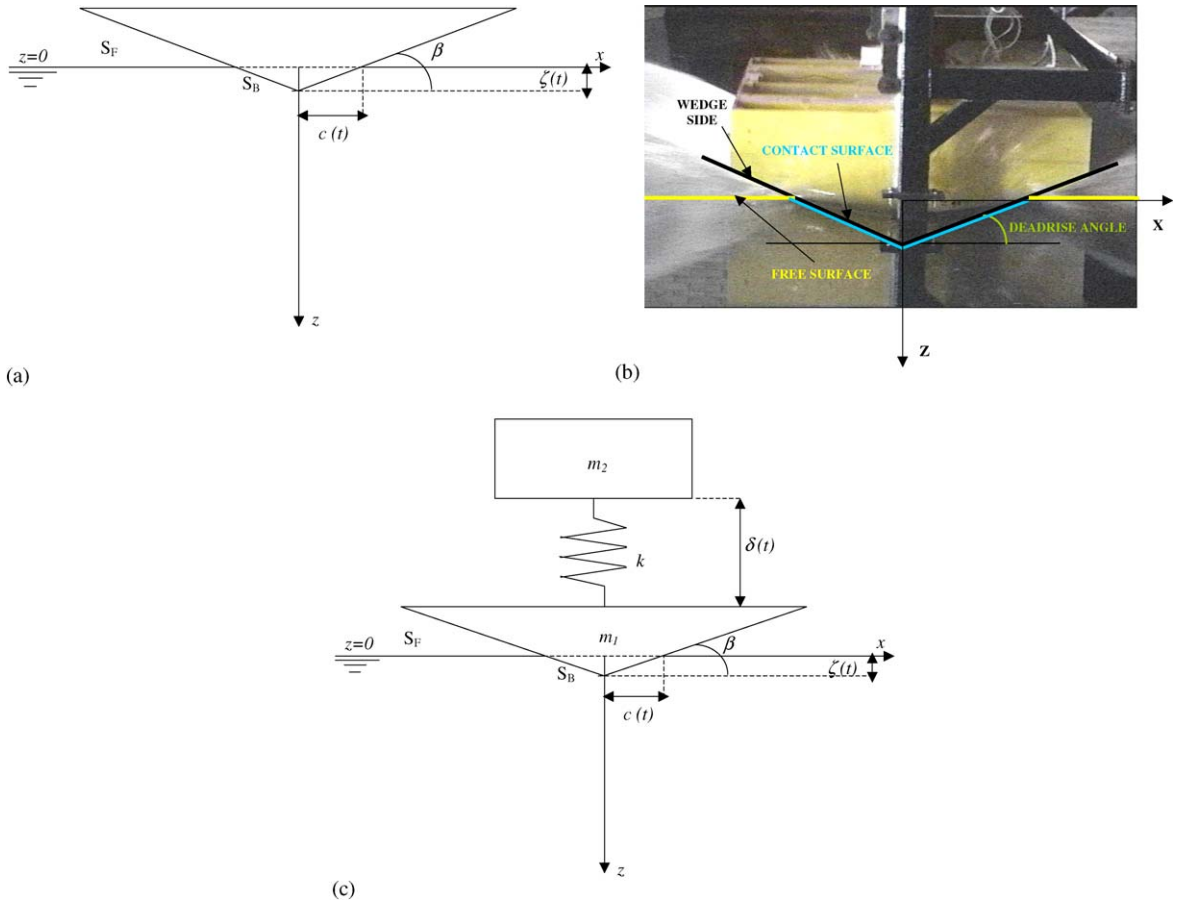

Fig. 3. (a) Sketch of the rigid impacting section and definition of the principal parameters. (b) Photograph of the front view of the wedge entering the free surface. Ideal contact surface, free surface and wedge sides. (c) Sketch of the ideal elastic oscillator plunging the water surface and definition of the principal parameters.

where F_h and ζ are the hydrodynamic force (per unit length) and the depth (positive downward), respectively.

First, a suitable form of the hydrodynamic force $F_h(\zeta, \dot{\zeta}, \ddot{\zeta})$ is obtained.

The problem of the impact looking at Figs. 3(a) and (b) is analyzed. The wedge is dropping along the z-axis (origin at the water plane), the x-axis lies on the water plane and the y-axis is orthogonal to the plane of the figure. Along this last direction the edge is supposed to have an infinite length. Moreover, the problem is symmetrical with respect to the z-axis and in addition the deadrise angle β is assumed to be small.

Two characteristic surfaces can be identified, the free water surface S_F and the water–body interface S_B. The formulation of the hydrodynamic problem follows the linearized Wagner approach [2]. In the pressure terms, derived by the Bernoulli equation, the non-linear contribution related to the squared velocity is in fact neglected. The kinematic conditions are also linearized, accounting for small perturbations of the surface S_F around the initial unperturbed configuration $z = 0$. The linearization finally allows the reduction of the contact surface to the segment $[-c, c]$ (see Figs. 3(a) and (b)), consistently with the hypothesis of β small.

However, in the present analysis, the Wagner model is generalized considering the variability of the wedge velocity during the impact [15,16]. Thus this model accounts for Eq. (1), being ignored in the original Wagner formulation. In fact, this is a crucial point to model the shock nature of the hydrodynamic force. To make the paper self-contained, some elements of the original Wagner theory are illustrated here.

When the fluid is supposed to be inviscid and an irrotational flow is assumed, a velocity potential $\phi(x, z, t)$ can be introduced, satisfying the well-known Laplace equation in the x, z plane.

The Laplace equation usually needs boundary values on the potential or on its normal derivatives, as in the classical problems of Dirichlet and Neumann, respectively. However, the present problem has moving boundaries: S_F is freely moving, while S_B is moving due to the side wedge kinematic constraint. Therefore additional unknowns, describing the surface configurations, must be introduced. S_F and S_B are described by the Cartesian equations $z = \eta(x, t)$ and $z = |x|\tan\beta - \zeta(t)$, respectively, being η and ζ the two further mentioned unknowns. Thus to solve the Laplace equation in the fluid domain, two additional equations are needed in terms of η, ζ and ϕ, besides the usual Neumann and Dirichlet conditions.

Moreover, the problem obeys the following initial conditions:

$$\phi(x, 0, 0) = 0, \quad \dot{\phi} = (x, 0, 0) = 0, \quad \zeta(0) = 0, \quad \dot{\zeta}(0) = v_0. \tag{2}$$

A zero pressure value is imposed on the free surface S_F thus: $p(x, \eta, t) = 0$, that, when using a linearized Bernoulli equation, leads to $\partial\phi(x, \eta, t)/\partial t = 0$. By using the initial conditions (2), this last equation becomes

$$\phi(x, \eta, t) = 0, \tag{3}$$

that is a Dirichlet condition. However the surface $z = \eta(x, t)$ on which this condition must be applied is unknown. A kinematic condition relating ϕ and $z = \eta(x, t)$ can be obtained in linearized form [19]

$$\frac{\partial\eta(x, t)}{\partial t} = \frac{\partial\phi(x, 0, t)}{\partial z}. \tag{4}$$

Now consider the boundary S_B. The kinematic constraint on the wedge sides implies the following linearized relationship:

$$\frac{\partial\phi(x,0,t)}{\partial z} = -\dot{\zeta} \tag{5}$$

that is a Neumann condition. However $\zeta(t)$ is unknown and must be determined by using the wedge equation of motion (1). In fact, the hydrodynamic force appearing in Eq. (1) is given by the integral of the pressure p over the water–body interface segment:

$$F_h(\zeta,\dot{\zeta},\ddot{\zeta}) = \int_{-c}^{c} p(x,0,t)\,\mathrm{d}x = -\int_{-c}^{c} \rho\frac{\partial\phi(x,0,t)}{\partial t}\,\mathrm{d}x.$$

Therefore, the sought additional relationship is obtained:

$$m\ddot{\zeta} = \int_{-c}^{c} \rho\frac{\partial\phi(x,0,t)}{\partial t}\,\mathrm{d}x. \tag{6}$$

Eqs. (3)–(6) are the four linearized boundary conditions associated with the Laplace equation with moving boundaries that, together with the given initial conditions (2), allow the determination of the set of unknowns represented by $c(t), \phi(x,z,t), \zeta(t)$ and $\eta(x,t)$.

In order to solve the posed problem, consider a Wagner-based solution generalized to the case in which the entry velocity is time dependent. Considering the analytic function

$$F(x+\mathrm{i}z) = \phi + \mathrm{i}\psi = -\mathrm{i}\dot{\zeta}\sqrt{(x+\mathrm{i}z)^2 - c^2(t)} - \dot{\zeta}z, \tag{7}$$

its real part ϕ has the properties:

it is harmonic, i.e., satisfies the Laplace equation in the x,z plane;

$$\phi(x,0,t) = \begin{cases} 0 & \text{for } |x| > c(t), \text{ i.e., on } S_F, \\ -\dot{\zeta}\sqrt{c(t)^2 - x^2} & \text{for } |x| < c(t), \text{ i.e., on } S_B, \end{cases}$$

$$\frac{\partial\phi}{\partial z}(x,0,t) = \begin{cases} \dfrac{\dot{\zeta}x}{\sqrt{x^2 - c(t)^2}} - \dot{\zeta} & \text{for } |x| > c(t), \text{ i.e., on } S_F, \\ -\dot{\zeta} & \text{for } |x| < c(t), \text{ i.e., on } S_B. \end{cases}$$

The boundary condition (5) is directly satisfied by this solution, as well as the boundary condition (3) in the frame of a linearized analysis, i.e., corresponding to the surface $z = 0$ instead of the actual one $z = \eta(x,t)$. To give explicit form to Eq. (6), first express the time derivative of $\phi(x,0,t)$ on S_B:

$$\frac{\partial\phi(x,0,t)}{\partial t} = -\ddot{\zeta}\sqrt{c^2 - x^2} - \dot{\zeta}\frac{c\dot{c}}{\sqrt{c^2 - x^2}}. \tag{8}$$

By substituting this result into Eq. (6), and integrating with respect to x, one has

$$m\ddot{\zeta} = -\pi\rho c\left[\ddot{\zeta}\,c/2 + \dot{\zeta}\dot{c}\right]. \tag{9}$$

A further equation relating $c(t)$ and $\zeta(t)$ is determined by integrating Eq. (4) with respect to time [2]. After some mathematics, it follows:

$$c(t) = \gamma \frac{\zeta(t)}{\tan\beta}, \tag{10}$$

where $\gamma = \pi/2$.

Eqs. (9) and (10) can be solved in terms of $c(t)$ and $\zeta(t)$. By substituting Eq. (10) into Eq. (9) a differential equation in terms of $\zeta(t)$ alone is determined:

$$\ddot{\zeta} + A\frac{\dot{\zeta}^2\zeta}{(1+\frac{1}{2}A\zeta^2)} = 0, \quad A = \frac{\pi\rho\gamma^2}{m\tan^2\beta}.$$

This equation admits a closed-form solution. Since the time t does not appear explicitly, the variable substitution $\dot{\zeta} = \psi(\zeta)$ is made, leading to the first order equation:

$$\frac{d\psi}{d\zeta}\psi + A\psi^2\frac{\zeta}{(1+\frac{1}{2}A\zeta^2)} = 0. \tag{11}$$

By separating the variables ζ and ψ, the solution $\psi(\zeta)$ is obtained as

$$\psi = \frac{C_0}{(2/A+\zeta^2)}, \tag{12}$$

being $C_0 = 2v_0/A$, when using the initial conditions (2). Thus, the previous equation becomes

$$\frac{d\zeta}{dt} = \frac{2v_0}{(2+A\zeta^2)},$$

that is again solved by separating the variables t and ζ, i.e.,

$$t(\zeta) = \frac{1}{6v_0}(A\zeta^3 + 6\zeta), \tag{13}$$

where the initial conditions (2) have been used. By inverting the previous relationship, one obtains three roots: two of them are complex and conjugate, while the third is real and has the following form:

$$\zeta(t) = -\frac{2}{\sqrt{A}\left(3\sqrt{A}tv_0 + \sqrt{8+9At^2v_0^2}\right)^{1/3}} + \frac{\left(3\sqrt{A}tv_0 + \sqrt{8+9At^2v_0^2}\right)^{1/3}}{\sqrt{A}}$$

that provides the sought after result.

Once $\zeta(t)$ is known, the time history of the hydrodynamic force is provided by Eq. (1).

In the original Wagner analysis, assuming $\zeta(t) = v_0 t$, only the set of Eqs. (3)–(5) is solved leading to the simpler expression $F_h = (\pi\gamma^2\rho/\tan^2\beta)v_0^3 t$ for the hydrodynamic force, that is a monotonically increasing function of the time t.

The mentioned characteristic value of the maximum hydrodynamic force F^* and the time t^* at which it occurs, can be also estimated in closed form. Since $\ddot{\zeta} = (d\psi/d\zeta)\psi$, from Eq. (11)

one obtains

$$\ddot{\zeta} = -Av_0^2 \frac{\zeta}{(1+\frac{1}{2}A\zeta^2)^3},$$

and considering the equation of motion (1):

$$F_h(\zeta) = m\ddot{\zeta} = -mAv_0^2 \frac{\zeta}{(1+(A/2)\zeta^2)^3}. \tag{14}$$

When solving the algebraic equation $\mathrm{d}F_h/\mathrm{d}\zeta = 0$, it follows

$$F^* = F_h(\zeta^*) = \left(\frac{5}{6}\right)^3 \frac{v_0^2}{\tan\beta}\sqrt{\frac{2\pi}{5}\rho\gamma^2 m}, \tag{15}$$

where ζ^* is the depth at which the maximum occurs. Moreover, by using Eq. (13), one has

$$t^* = t(\zeta^*) = \frac{16}{15}\sqrt{\frac{2m}{5\pi\rho\gamma}}\frac{\tan\beta}{v_0},$$

and

$$\zeta^* = \tfrac{15}{16} v_0 t^*.$$

Finally, simple mathematics leads to $F^*t^* = \frac{20}{81}mv_0 \approx 0.247mv_0$.

Even though the determined equations could be directly employed to provide the shock hydrodynamic force, a more general and even simpler result can be obtained by introducing a suitable non-dimensional form of the hydrodynamic load, useful in the following. If Eq. (14) is rewritten in terms of non-dimensional variables: $\tilde{t} = t/t^*, \tilde{\zeta} = \zeta/\zeta^*, \tilde{F}_h = F_h/F^*$, the hydrodynamic force takes the form below:

$$\tilde{F}(\tilde{t}) = \frac{81}{20b}\left[\frac{2}{2+\tilde{\zeta}^2/b}\right]^3 \tilde{\zeta}, \quad \tilde{\zeta}(\tilde{t}) = -\frac{2}{\sqrt{2\gamma/5}Q^{1/3}} + \frac{Q^{1/3}}{\sqrt{2\gamma/5}},$$
$$Q(\tilde{t}) = 3a\tilde{t}\sqrt{8+(3a\tilde{t})^2}, \quad a = \sqrt{2\gamma/5}\,\tfrac{16}{15}, \quad b = \tfrac{5}{2}\left(\tfrac{15}{16}\right)^2. \tag{16}$$

Eqs. (16) show that the slamming force is invariant with respect to the impact parameters when this particular non-dimensional form is chosen. This allows an analysis that is not case dependent. Actually, a single time history of the hydrodynamic force is determined, being each possible impact case determined by suitably scaling the force and time axes. The curve given by Eq. (16) is represented in Fig. 4.

In the previous analysis γ is constant. However, more accurate investigations of this point [20] show that this is accurate only when the deadrise angle tends to zero. When the above assumption does not strictly hold, a dependency of γ on β must be assumed. In the following it is implicitly considered $\gamma = \gamma(\beta)$ assuming the correlation given in Ref. [15].

Some comments and comparisons with the method presented in Ref. [14] are needed. In fact in that work, the analysis of the impact of a rigid body is made following the Vorus approach [10] to describe the hydrodynamic load. The model, as mentioned in the introduction, retains non-linear terms in the Bernoulli equations and includes two impact phases: chine dry and chine wet; this last stage is not considered in the present investigation. However, in the frame of an analysis limited to

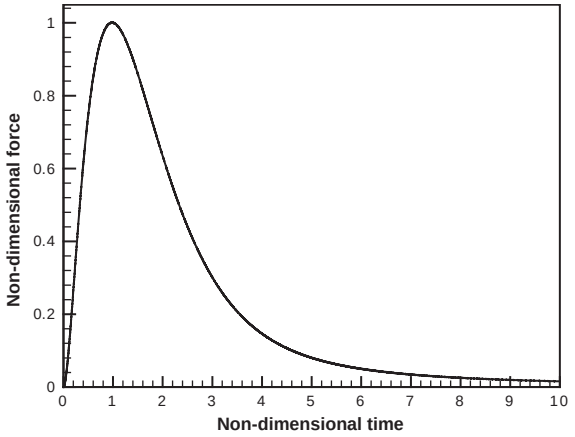

Fig. 4. Non-dimensional time history of the hydrodynamic force.

the chine dry phase, the results are in satisfactory agreement with those obtained by experiments (see Section 5) even by considering the simplified Wagner model. The advantage relies on the closed-form results given by Eqs. (16). In more depth, a direct comparison between the numerical results in Ref. [14] and the equations obtained in the present work is possible. In Ref. [14] the dimensionless parameters are introduced: $\alpha = m/\rho B^2$ and $\tilde{\ddot{y}} = \ddot{\zeta}B/4gH$; B is the wedge beam at the chine and H is the drop height ($v_0 = \sqrt{2gH}$). On the basis of numerical simulations it is argued in Ref. [14] that when the mass is small the maximum acceleration is large. This result finds a strict foundation (neglecting the buoyancy force) on the basis of Eq. (15): by substituting into it $m = \alpha\rho B^2$ and $\tilde{\ddot{y}}_{max} = \ddot{\zeta}_{max}B/4gH = F^*B/4gHm$, one has

$$\tilde{\ddot{y}}_{max} = (\tfrac{5}{6})^3 \frac{\gamma}{\tan\beta}\sqrt{\frac{\pi}{10\alpha}},$$

disclosing the analytical dependence between the peak acceleration and the beam loading parameters. It appears that $\tilde{\ddot{y}}_{max}(\alpha)$ depends only on the deadrise angle β.

Finally in Ref. [14] the relationship between the non-dimensional time $\tau_{max} = v_0 t^*/(B/2)$, corresponding to the maximum acceleration, and the beam loading α is numerically investigated concluding that τ_{max} increases when α increases. Eq. (16) provides a strict support to this statement. After some mathematics $\tau_{max}(\alpha)$ is determined as

$$\tau_{max} = \left(\tfrac{40}{81}\right)\left(\tfrac{6}{5}\right)^3\left(\tfrac{5}{2\pi}\right)^{1/2}\frac{\tan\beta}{\gamma}\sqrt{\alpha}.$$

Again, it appears that $\tau_{max}(\alpha)$ depends only on the deadrise angle.

Of course, these comparisons are valid in the limit of the chine dry condition that means $\zeta < B\tan\beta/2$.

2.2. Elastic response to the hydrodynamic shock

In the following two sections the response of an elastic system carried on-board the impacting wedge is analyzed. In Section 2.2.1 a single-d.o.f. oscillator is considered, while in Section 2.2.2 the

case of an elastic free–clamped beam is investigated. The second case is examined in view of a better understanding of the experimental analysis presented in Section 4, where, for the sake of simplicity of the experimental set up, the actual elastic system on board is realized by a variable length beam.

2.2.1. The single-d.o.f. system response to the hydrodynamic shock

A simple system, consisting of two elastically coupled bodies of mass m_1 and m_2 is investigated here. The lower one, a rigid wedge with mass m_1, directly impacts the water, while the upper is suspended over the first one by a spring of stiffness k (Fig. 3c).

Although this is an elementary structure, it can be investigated as a prototype system whose behaviour reveals of important characteristics of the structural water shock response.

The equations of motion of the system are

$$\begin{aligned} m_1\ddot{\zeta} &= -F_h(\zeta,\dot{\zeta},\ddot{\zeta}) + F_e(\delta), \\ m_2(\ddot{\zeta}+\ddot{\delta}) &= -F_e(\delta), \end{aligned} \tag{17}$$

where δ is the relative displacement between the two masses and $F_e(\delta) = k\delta$ is the elastic force due to the spring. Since in the previous section the evaluation of the hydrodynamic force was obtained, it is interesting to study under which conditions this force is almost independent of the elastic force, i.e., when the motion of m_1 is substantially independent of the motion of m_2. In such a case the hydrodynamic force analysis, developed in Section 2.1, is still valid.

A very simple criterion to identify when this hypothesis holds can be given. The maximum elastic force in the spring should be much smaller than the maximum hydrodynamic force. The former can be estimated by considering the limit case in which the whole impact kinetic energy $\frac{1}{2}m_2v_0^2$ of the suspended mass is completely converted into elastic energy $\frac{1}{2}m_2\delta^2$ (corresponding to consideration of an instantaneous stop of the wedge due to the impact). The latter force is naturally estimated by F^* given in Eq. (15). When the elastic force $F_e = \sqrt{m_2v_0^2k}$, evaluated with the previous criterion, satisfies the condition $F_e \ll F^*$, the following inequality holds:

$$\frac{1}{\gamma^2}\tan^2\beta\mu\frac{k}{\rho v_0^2} \ll 1.$$

Under this hypothesis the suspended mass behaves reasonably like a mass on a foundation that receives a known shock acceleration of the form $F_h(t)/m_1$. In this case system (17) reduces to the simpler form

$$\begin{aligned} m_1\ddot{\zeta} &= -F_h(\zeta,\dot{\zeta},\ddot{\zeta}), \\ \ddot{\delta} + \omega_n^2\delta &= -\ddot{\zeta}, \end{aligned} \tag{18}$$

being ω_n the natural frequency of the carried mass m_2 when m_1 is blocked. Thus the first equation is independent of the second and it is solved as shown in Section 2.1. Once the depth ζ of the wedge is determined, the second equation can be solved, being $\ddot{\zeta}$ a known force term.

Now examine the problem of finding a critical value of the stiffness k, i.e., the value that leads to the maximum amplitude of the spring elastic force, once all the other impact parameters are given. The maximum of this last quantity also corresponds to the maximum of the absolute

acceleration of the carried mass, since elastic force and absolute acceleration are obviously proportional.

Since the hydrodynamic force has a pulse nature and the maximum elastic force response of the system is of interest, the shock spectrum technique can be profitably used. The following analyzes this point in detail.

Using the equation of motion, the response of the carried mass is described by the convolution integral as

$$\delta(t) = -\int_0^t \ddot{\zeta}(\tau)\frac{1}{\omega_n}\sin\omega_n(t-\tau)\,\mathrm{d}\tau.$$

The interest of this study is to evaluate the residual elastic response, i.e., the response for large values of t. Since the hydrodynamic force has a transient nature, for t large the hydrodynamic force is almost zero. This means

$$\ddot{\zeta}(t)\to 0 \quad \text{for} \quad t\to\infty.$$

In practice, this condition holds for $t > 8$–$10t^*$. After this time the carried mass behaves as a freely oscillating system whose residual motion can be described by $\delta(t) = \Delta_{\mathrm{res}}\sin(\omega_n t + \psi)$, where Δ_{res} is the amplitude of the residual elastic vibration and ψ a suitable phase angle. Under the hypothesis $t\to\infty$, the previous convolution integral becomes:

$$\Delta_{\mathrm{res}}\sin(\omega_n t + \psi) = -\int_{-\infty}^{\infty}\ddot{\zeta}(\tau)\frac{1}{\omega_n}\sin\omega_n(t-\tau)\,\mathrm{d}\tau,$$

where the lower integral limit $t = 0$ is replaced by $t = -\infty$, because for $t<0$, the wedge has a uniform motion characterized by $\ddot{\zeta}(t) = 0$. By using the previous relationship and its time derivative, the following complex equation is easily obtained:

$$\Delta_{\mathrm{res}}\mathrm{e}^{\mathrm{j}\psi} = -\frac{1}{\omega_n}\int_{-\infty}^{\infty}\ddot{\zeta}(\tau)\mathrm{e}^{-\mathrm{j}\omega_n\tau}\,\mathrm{d}\tau,$$

providing the vibration response $\Delta_{\mathrm{res}}\mathrm{e}^{\mathrm{j}\psi}$ (amplitude and phase) of the carried mass. Thus the complex elastic force is

$$F_{\mathrm{res}}\mathrm{e}^{\mathrm{j}\psi} = k\Delta_{\mathrm{res}}\mathrm{e}^{\mathrm{j}\psi} = -m_2\omega_n\int_{-\infty}^{\infty}\ddot{\zeta}(\tau)\mathrm{e}^{-\mathrm{j}\omega_n\tau}\,\mathrm{d}\tau.$$

The integral on the right side is the Fourier transform F of the wedge acceleration during the impact, being its argument equal to the circular natural frequency of the elastic system, i.e.,

$$F_{\mathrm{res}}(\omega_n) = m_2\omega_n|\mathrm{F}\{\ddot{\zeta}\}|_{\omega=\omega_n}|,$$

or by introducing the hydrodynamic force

$$F_{\mathrm{res}}(\omega_n) = \mu\omega_n|\mathrm{F}\{F_h\}|_{\omega=\omega_n}|, \tag{19}$$

Looking at the dependency of the force on ω_n, critical impact conditions can be defined on the basis of a relative maximum in the previous function, i.e.,

$$\omega_n|\mathrm{F}(\omega_n)| + \frac{\mathrm{d}|\mathrm{F}(\omega_n)|}{\mathrm{d}\omega_n} = 0.$$

Thus the critical natural frequency of the elastic system is the solution of the previous equation.

By using the non-dimensional variables $\tilde{t}, \tilde{\zeta}$ and $\tilde{F}_h$ introduced in Section 2.1 combined with Eq. (19), one obtains

$$\tilde{F}_{\mathrm{res}}(\tilde{\omega}_n) = \mu\tilde{\omega}_n \left| \int_{-\infty}^{\infty} \tilde{F}_h(\tilde{\tau}) \mathrm{e}^{-\mathrm{j}\tilde{\omega}_n\tilde{\tau}} \, \mathrm{d}\tilde{\tau} \right|, \quad \text{i.e., } \tilde{F}_{\mathrm{res}}(\tilde{\omega}_n) = \mu\tilde{\omega}_n |\mathrm{F}\{\tilde{F}_h(\tilde{\tau})\}|\tilde{\omega} = \tilde{\omega}|. \tag{20}$$

It is apparent by Eqs. (16) that $\tilde{F}_h(\tilde{t})$ is a function of $\tilde{t}$ only and that its Fourier transform, appearing in Eq. (20), is just a function of $\tilde{\omega}_n$. Thus, it can be concluded that, whatever the physical parameters of the impact problem, the intensity of the elastic residual force is only function of $\tilde{\omega}_n$ and μ. Moreover, this functional dependency is easily determined by simply computing the Fourier transform of $\tilde{F}_h(\tilde{t})$ given by Eq. (16), i.e., by evaluating the function $\mathrm{F}\{\tilde{F}_h(\tilde{\tau})\}$ that can be determined, irrespectively of the particular analysed impact case.

As a consequence, all the possible elastic residual forces can be represented by a simple family of curves having their relative maximum at the same dimensionless frequency, being the maximum amplitude proportional to μ. More simply, the single function $\tilde{F}_{\mathrm{res}}(\tilde{\omega}_n)/\mu$ is represented versus the non dimensional frequency $\tilde{f}_n = f_n t^* = \omega_n t^*/2\pi$. This curve, represented in Fig. 5 (dotted line), is the residual shock spectrum of the elastic force (or, equivalently, the residual shock spectrum of the absolute acceleration of the carried mass). The actual elastic force can be determined by multiplying the residual force by the maximum hydrodynamic force F^* and by the mass factor $\mu = m_2/m_1$. By direct inspection of the shock spectrum curve, it appears that the relative maximum occurs at $\tilde{f}_n \cong 0.2$ and, hence, the critical frequency can be estimated as

$$\tilde{f}_{\mathrm{cr}} = (f_n t^*)_{\mathrm{cr}} \approx 0.2.$$

Although simplification hypotheses are introduced, this is a general result. In fact, since t^* has been determined analytically in Section 2.1, a simple and effective expression holds:

$$f_{n\mathrm{cr}} \approx \frac{3}{16}\sqrt{\frac{5\pi\rho\gamma}{2m_1}} \frac{v_0}{\tan\beta} \tag{21}$$

providing the critical natural frequency—and also the desired value of the critical stiffness k—of the carried elastic system when all the impact parameters are given. Looking at Fig. 5, it appears

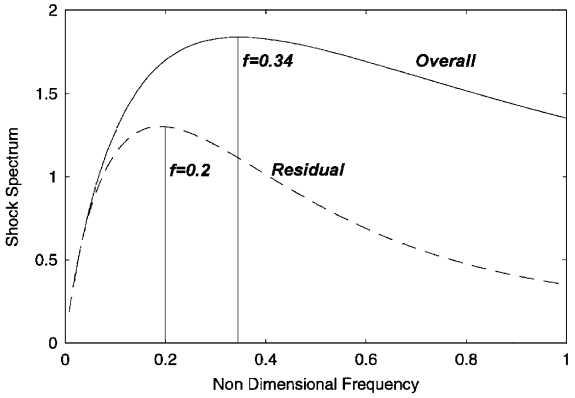

Fig. 5. Non-dimensional residual and overall shock spectra.

that, corresponding to this frequency, the amplitude of the elastic force has the maximum residual value:

$$F_{\text{res}} \approx 1.3\ \mu\ F^* = 1.3\ \mu\ \left(\frac{5}{6}\right)^3 \frac{v_0^2}{\tan\beta}\sqrt{\frac{2\pi}{5}\rho\gamma^2 m_1}. \tag{22}$$

It should be added that the asymptotic residual response does not necessarily provide the maximum vibrational amplitude of the system during the transient excitation, but only the asymptotic one. To this aim the overall shock spectrum must be determined. This requires the direct evaluation of the absolute maximum of the elastic response. The solution of the second of Eqs. (18), since $\delta(0) = 0,\ \dot{\delta}(0) = 0$, is simply expressed by using the Fourier transform

$$\mathrm{F}\{\delta\} = -\frac{\mathrm{F}\{\ddot{\zeta}\}}{\omega_n^2 - \omega^2} \quad \rightarrow \quad \delta(t) = -\frac{1}{2\pi}\int_{-\infty}^{+\infty} \frac{\mathrm{F}\{\ddot{\zeta}\}}{\omega_n^2 - \omega^2}\, \mathrm{e}^{\mathrm{j}\omega t}\, \mathrm{d}\omega.$$

By introducing the previously defined non-dimensional quantities, after simple mathematics, the dimensionless elastic force $\tilde{F}_e = -k\delta/F^*$ is obtained:

$$\tilde{F}_e(\tilde{t},\tilde{f}_n) = \mu \int_{-\infty}^{+\infty} \frac{\mathrm{F}\{\tilde{F}_h\}}{[1-(\tilde{f}/\tilde{f}_n)^2]}\, \mathrm{e}^{2\pi \mathrm{j}\tilde{f}\tilde{t}}\, \mathrm{d}\tilde{f}. \tag{23a}$$

Even in this case a single characteristic curve is determined, able to deal with any impact condition. Thus, the slamming overall shock spectrum is determined as

$$\max\{\tilde{F}_e(\tilde{t},\tilde{f}_n)\}, \quad 0 \leqslant t < \infty. \tag{23b}$$

Again the actual elastic force is determined as a function of the amplitude factor $F^*\mu$. This characteristic function has been evaluated and plotted in Fig. 5. Its relative maximum corresponds to

$$\tilde{f}_{\text{cr}} = (f_n t^*)_{\text{cr}} = 0.34,$$

and the maximum amplitude of the overall elastic force is

$$F_{\text{ov}} \approx 1.8\mu F^*.$$

Eqs. (20)–(23b) represent the central theoretical result of this paper.

It is apparent that both the maximum residual and overall elastic forces have the same order of magnitude as the hydrodynamic one, when the mass factor μ is of unit order of magnitude, being $F_{\text{res}} \approx 1.3\mu F^*$, $F_{\text{ov}} \approx 1.8\mu F^*$. Since the initial assumption requires $F_h \gg F_e$, the developed analysis is valid under the assumption that μ is small.

A final remark concerns the presence of damping in the carried oscillator that has not been considered in the previous analysis. This point has a certain importance since, in practice, damping is always present, as in the experiments that will be presented later to validate the theoretical analysis. While damping does not affect significantly the overall response of the system, simply leading to a weak reduction of the predicted maximum peak (at least for small damping), this must be explicitly considered when dealing with the residual response. Since damping implies indeed an exponential reduction of the response amplitude, the concept of the residual response, intended as the stationary amplitude vibration after the load vanishes, becomes meaningless.

In this case the residual force—obtained for t large—is a decaying signal $F_{\text{res}}e^{-\chi t}e^{j\psi}$, where the coefficient χ accounts for the dissipation effects. Thus the force amplitude is not constant anymore. Nevertheless, to obtain a significant estimate of the system's excitation due to the external shock, the new quantity can be considered:

$$R = \frac{1}{\Delta T}\int_{T}^{T+\Delta T} |F_{\text{res}}(t)|\mathrm{d}t, \tag{24}$$

providing a measure of the average elastic force generated by the shock over a given time interval ΔT once its energy vanishes (i.e., $T \approx 8$–$10t^*$). On this basis, the previous procedure modifies slightly. The residual response is now

$$\Delta_{\text{res}}e^{-\chi t}\sin(\omega_n t + \psi),$$

leading to the elastic force in complex form:

$$F_{\text{res}}(t) = F_{\text{res}}e^{-\chi t}e^{j\omega_n t}e^{j\psi} = k\Delta_{\text{res}}e^{-\chi t}e^{j\omega_n t}e^{j\psi}.$$

Therefore, the sought integral is

$$R = \frac{1}{\Delta T}\int_{T}^{T+\Delta T} |F_{\text{res}}(t)|\,\mathrm{d}t = \frac{e^{-\chi T}(1-e^{-\chi\Delta T})}{\chi\Delta T}k\Delta_{\text{res}}.$$

The last term $F_{\text{res}}(\omega_n) = k\Delta_{\text{res}}$, is the residual amplitude force in absence of damping, i.e., it can be calculated as in Eq. (19). The obtained result shows that in presence of damping, by using definition (24), the correction factor $e^{-\chi T}(1-e^{-\chi\Delta T})/\chi\Delta T$ must be introduced. This term depends, in general, on the frequency (actually χ is frequency dependent) affecting the trend of the residual shock spectrum $F_{\text{res}}(\omega_n) = k\Delta_{\text{res}}$. However, at least assuming χ linearly dependent on the frequency (viscous damping), the correction factor introduces in the shock spectrum, besides an obvious reduction of the amplitude, a decreasing trend as the frequency increases: this produces a shifting of the shock spectrum peak towards the low frequencies. Thus, at least for light damping, a small reduction of the critical frequency, in comparison with that given by Eq. (21), is expected and Eq. (21) can be considered a good approximation of the desired results.

The numerical analysis proposed in Ref. [14] suggests that an appropriate selection of the mass/stiffness parameters allows a reduction of the suspended body acceleration. In the present work the problem of the general relationship between the body acceleration and mass/stiffness parameters finds a closed form solution expressed by Eqs. (20)–(23b). However, it is important to recall that this is possible under the following hypotheses: (i) chine wet conditions are not reached; (ii) the elastic force is small compared with the hydrodynamic one; (iii) the mass ratio μ is small. In Ref. [14] the numerical simulations refer to the values $\mu = 1$ and 10 that fall outside the admissible range for μ considered in the present paper: thus for this case direct comparisons are not possible.

2.2.2. The beam response to the hydrodynamic shock

For the sake of simplicity in the experimental realization, the elastic system on board is a simple free–clamped beam (see Section 4). In the previous section the absolute acceleration of the carried mass—that is equal to the elastic force—has been investigated. Analogously, the absolute acceleration response $a(t)$ of the beam end is considered. The maximum value of $a(t)$, and the natural frequency of the beam leading to this critical impact condition, is predicted by a shock-

spectrum approach similar to that presented in the previous section. The main difference with respect to the simpler single-d.o.f. model, is that the actual beam structure responds, in general, with an infinite number of modes. Moreover the beam's natural frequencies are modified by varying its length, i.e., its total mass. Thus, a specific analysis of the beam's shock spectrum response is necessary.

Although a residual shock analysis could be developed accounting for the complete modal expansion [15], more complex analysis is not necessary, because even the single-mode approximation leads to a satisfactory agreement with the experimental measurements.

Considering only the first mode response $w(x,t) = \phi_1(x)q_1(t)$ of the beam, one has

$$EI\frac{\partial^4 w}{\partial x^4} = -\rho S\left(\frac{\partial^2 w}{\partial t^2} + \ddot{\zeta}\right) \quad \rightarrow \quad EI\phi_1^{\mathrm{IV}} q_1 = -\rho S(\phi_1 \ddot{q}_1 + \ddot{\zeta}), \tag{25}$$

where ϕ_1, q_1, ω_{n1}, ρ, S, E, I are the first mode shape, the Lagrangian co-ordinate, the first natural frequency, the mass density, the cross sectional area, Young's modulus and the moment of inertia of the beam, respectively.

For convenience let $\phi_1(x) = \Gamma\tilde{g}(\xi)$, where $\tilde{g}(\xi)$ is the dimensionless mode shape function and $\xi = x/l$; since $\phi_1(x)$ satisfies an orthonormality condition, it follows

$$\Gamma = \frac{1}{\sqrt{\rho S l}} \frac{1}{\sqrt{\int_0^1 \tilde{g}^2(\xi)\,\mathrm{d}\xi}}. \tag{26}$$

Moreover the mode $\tilde{g}(\xi)$ satisfies the equation

$$\frac{\mathrm{d}^4\tilde{g}}{\mathrm{d}\xi^4} = \lambda^4\tilde{g}, \tag{27}$$

where, for the clamped–free beam, $\lambda = 1.875$. The absolute acceleration $a(t)$ at the beam's end is

$$a(t) = \phi_1(l)\ddot{q}_1(t) + \ddot{\zeta}(t).$$

Thus, by combining Eqs. (25) and (27), one obtains

$$a(t) = -\tilde{g}(1)\omega_{n1}^2\Gamma q_1(t). \tag{28}$$

This demonstrates that the absolute acceleration at the beam's end is proportional to the Lagrangian co-ordinate.

First evaluate the residual response a_{res}. The Lagrangian co-ordinate satisfies the equation

$$\ddot{q}_1(t) + \omega_{n1}^2 q_1(t) = \Pi, \quad \Pi = -\rho S\int_0^l \phi_1\,\mathrm{d}x\ddot{\zeta}, \tag{29}$$

that is formally equivalent to Eq. (18), $\ddot{\delta} + \omega_n^2\delta = -\ddot{\zeta}$, except for the value of the appearing coefficient on the right side. In fact, in this case, the forcing term depends on the beam length l, i.e., on the beam's first natural frequency. Following an analysis identical to that shown in Section 2.2.1, one obtains

$$t \rightarrow \infty, \quad q_1(t) = q_{\mathrm{res}}\mathrm{e}^{\mathrm{j}\omega_{n1}t}\mathrm{e}^{\mathrm{j}\psi},$$

$$q_{1\mathrm{res}}(\omega_{n1}) = -\frac{\Pi}{\omega_{n1}}|\mathrm{F}\{\ddot{\zeta}\}||_{\omega=\omega_{n1}},$$

where $q_{1\mathrm{res}}(\omega_{n1})$ is the residual value of the Lagrangian co-ordinate and ψ a suitable phase angle. On the basis of the last equation and of Eq. (28), the beam's end residual acceleration is

$$a_{\mathrm{res}}(\omega_{n1}) = \tilde{g}(1)\Gamma\Pi\omega_{n1}|\mathrm{F}\{\ddot{\zeta}\}||_{\omega=\omega_{n1}}, \quad \Gamma\Pi = \frac{\int_0^1 \tilde{g}\,\mathrm{d}\xi}{\int_0^1 \tilde{g}^2\,\mathrm{d}\xi}, \tag{30}$$

that is identical to expression (19) when replacing the dimensionless factor μ with the dimensionless factor $\tilde{g}(1)\Gamma\Pi$, that depends only on the chosen boundary conditions (free–clamped), while it is at all independent of the beam's natural frequency. Therefore, also in this case, the maximum of a_{res} is predicted at $\tilde{f}_{\mathrm{cr}} = (f_n t^*)_{\mathrm{cr}} \approx 0.2$. It is remarked how the same conclusion is drawn for the residual relative acceleration $\ddot{w}(l,t)$. In fact, since the residual response by definition is obtained when the exciting force vanishes, i.e., for $F_{w\mathrm{res}} = m_1\ddot{\zeta}_{\mathrm{res}} \approx 0$, it follows:

$$a(t) = \ddot{w}(l,t) + \ddot{\zeta}(t) \quad \rightarrow \quad a_{\mathrm{res}}(\omega_{n1}) = \ddot{w}_{\mathrm{res}}(l,\omega_{n1}).$$

Now analyze the overall response. The solution of Eq. (29), considering the initial conditions $q_1(0) = 0$, $\dot{q}_1(0) = 0$, is obtained by the Fourier transform technique:

$$\mathrm{F}\{q_1\} = -\Pi\frac{\mathrm{F}\{\ddot{\zeta}\}}{\omega_{n1}^2 - \omega^2} \quad \rightarrow \quad q_1(t) = -\Pi\frac{1}{2\pi}\int_{-\infty}^{+\infty}\frac{\mathrm{F}\{\ddot{\zeta}\}}{\omega_{n1}^2 - \omega^2}\mathrm{e}^{\mathrm{j}\omega t}\,\mathrm{d}\omega.$$

When using Eq. (28), the overall shock spectrum of a is

$$a(t) = \tilde{g}(1)\Pi\Gamma\frac{1}{2\pi}\int_{-\infty}^{+\infty}\omega_{n1}^2\frac{\mathrm{F}\{\ddot{\zeta}\}}{\omega_{n1}^2 - \omega^2}\mathrm{e}^{\mathrm{j}\omega t}\,\mathrm{d}\omega, \quad \max\{a(t)\} \quad 0 \leqslant t < \infty. \tag{31}$$

These last expressions, turned to a dimensionless form, are identical to Eqs. (23a) and (23b) where μ is substituted by $\tilde{g}(1)\Gamma\Pi$. Thus, also for the beam's case, the overall acceleration response is expected at $\tilde{f}_{\mathrm{cr}} = (f_n t^*)_{\mathrm{cr}} = 0.34$.

Finally, the presence of damping is dealt by Eq. (24) where the force is replaced by the absolute acceleration.

3. Design of the experimental set up

An experimental apparatus was designed to perform slamming tests and to validate the theoretical results shown in the previous sections.

The tests are aimed to measure the time history of the hydrodynamic force on the wedge and the response of the elastic system on board. Moreover the experimental reproduction of the residual and overall shock curves, given by the shock spectrum approach, is performed.

The theoretical model so far considered in Section 2.1 is based on the following main assumptions:

(a) the fluid is incompressible and inviscid, the flow irrotational and the free surface is initially at rest; no air entrapping effects are included in the theory;
(b) the wedge is assumed infinite along the y-axis (3D effects are not included in the theory);
(c) the fluid domain is infinite along both x- and y-axis and an infinite depth is assumed;
(d) the problem is symmetrical with respect to the zy plane.

The experimental set up was designed with the aim of meeting as closely as possible the conditions mentioned.

Concerning point (a), the experiments are performed in still water that behaves incompressibly at least for a deadrise angle which is not too small [21]. Moreover, the deadrise angle must be large enough also to limit air entrapping effects and dangerous stress in the impacting structure. On the other hand, the linearization of the body boundary conditions (Section 2.1) and the substitution of the actual contact surface with the segment $[-c, c]$, implies that the deadrise angle must be small.

The choice of an angle $\beta = 30^\circ$ (see Fig. 3(b)) used in the experimental tests, is a compromise between these opposite requirements.

To avoid three-dimensional effects mentioned in (b), some preliminary considerations about the characteristic sizes of the impacting body are needed. The basic requirement is the design of a wedge that can be considered almost infinite in the direction y parallel to the keel. This condition is satisfied in practice when the ratio between the characteristic wetted lengths L and $c(t)$ of the wedge along y and x, respectively, is large enough. It is shown in Ref. [16] that a ratio $L/c(t) > 3$ reduces largely undesired three-dimensional effects. This consideration is used for a correct choice of the wedge length L. In fact, by considering expression (10) of $c(t)$ in correspondence of the characteristic time t^*, i.e., $c(t^*) = \gamma\zeta^*/\tan\beta = \sqrt{2m/(5\pi\rho\gamma)}$, it is possible to estimate the ratio $L/c(t)$ when the maximum hydrodynamic force is reached. While the force is independent of the entry velocity, it depends on the mass per unit length of the wedge, $m = 45$ kg/m in the experimental configuration. It follows that when the keel length is $L = 160$ cm, the ratio $L/c(t^*)$ is about 25. If the analysis is performed for a longer time, e.g., the time needed for the hydrodynamic force to vanish ($t > 8$–$10t^*$), the length ratio goes down till a value of about 5.

About point (c), the experiments are performed in a towing tank with depth and width 3.5 and 12 m, respectively, and the side of the wedge is 2 m from by the tank wall. This configuration allows the avoidance of significant surface wave reflections, at least in the time interval during which the impact phenomenon is observed. Moreover with a depth of 3.5 m any disturbance effect due to the tank floor is negligible.

The symmetry requirement (d), suggests the guidance of the wedge during the falling run by a pair of rails. In fact, it is difficult to obtain a sharp trim control using a free falling device. This is mainly due to the wedge release phase that can induce non-zero pitch and roll angles leading to a non symmetrical impact. However, the guide rails can also introduce some errors on the measured hydrodynamic force. Part is related to kinematic errors, due to the rail positioning and clearances that can affect the roll and the pitch angles, part to dynamic effects due to the presence of rail reactions.

The designed rig has a maximum vertical run of 3 m so that the wedge, made of wood, attached to a supporting bar, can fall from variable heights leading to different entry velocities. The maximum value of the entry velocity is related to the maximum acceleration, which in order to keep the integrity of the structure and the instruments, cannot be higher than 25–30 g. The drop height range used in the experiments is $0.25 \leqslant h \leqslant 2$ m, roughly corresponding to an impact velocity range $1.5 \leqslant v_0 \leqslant 5$ m/s. In Fig. 6 the picture of the experimental apparatus is shown, and a view of an impact is given in Figs. 1 and 2.

The design of the elastic structure on board is now discussed. The elastic system consists of a clamped–free beam, where the clamped end is attached to the wedge. The shock spectral analysis

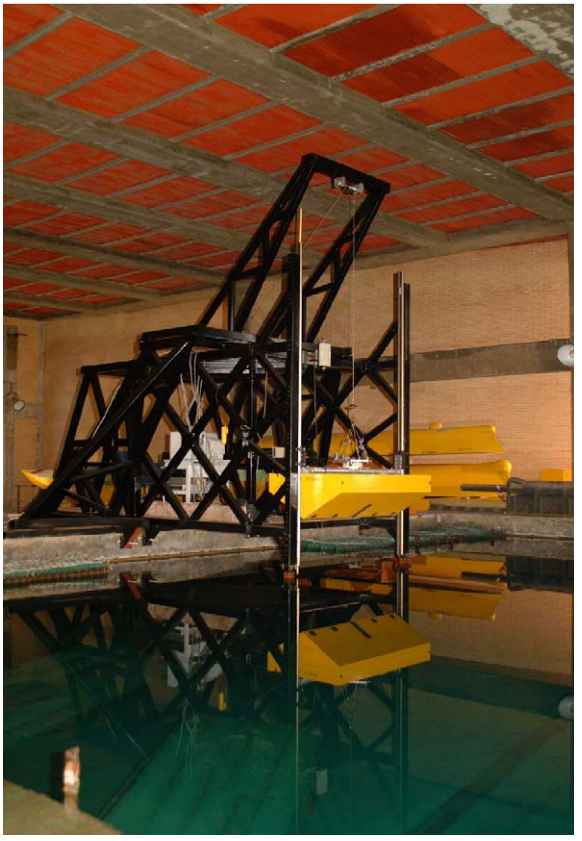

Fig. 6. View of the experimental facility; the supporting frame and the wedge running on vertical rails.

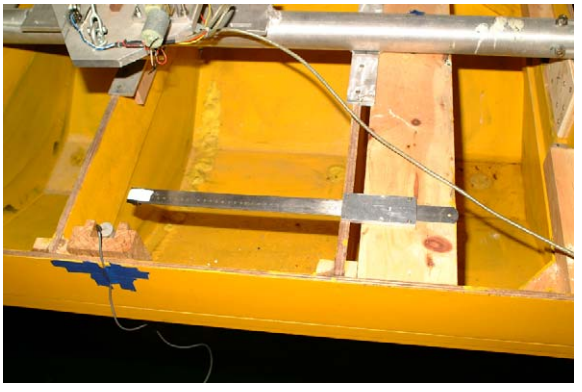

Fig. 7. View of the elastic beam mounted on board of the wedge (note on the left the accelerometer attached to the wedge).

needs to investigate the response of the elastic system when varying its natural frequency. Thus the beam clamp is realized by a vice, so that the beam's length can be varied (see Fig. 7) and the first natural frequency of the beam can be modified within a suitable range.

Looking at Fig. 5, the overall experiments must follow the trend of the shock spectrum curves about the critical values of the non-dimensional frequency 0.34. Actually a non-dimensional frequency range 0.05–0.8 has been selected for the experimental investigation. This implies that $0.05 \leqslant \tilde{f} = f_n t^* \leqslant 0.8$. Given a characteristic time $t^* = 0.024$, corresponding to the test condition mass = 46 kg/m, $v_0 = 2.2$ m/s, $\beta = 30^\circ$, the first natural frequency of the beam must be $3.65 \text{ Hz} \leqslant \tilde{f} = f_{n1} t^* \leqslant 73.5$ Hz.

Finally, for the residual shock spectrum, the critical non-dimensional frequency is 0.24 and the non-dimensional frequency range 0.0876–0.66 was investigated. The corresponding range for the beam natural frequency is $5.2 \leqslant f_n \leqslant 27.5$ Hz. The analysis of the residual response is more difficult compared with the overall response. In fact, as shown in Section 2.2, the residual response is more sensitive to damping effects. When using an accelerometer to measure the beam end acceleration,

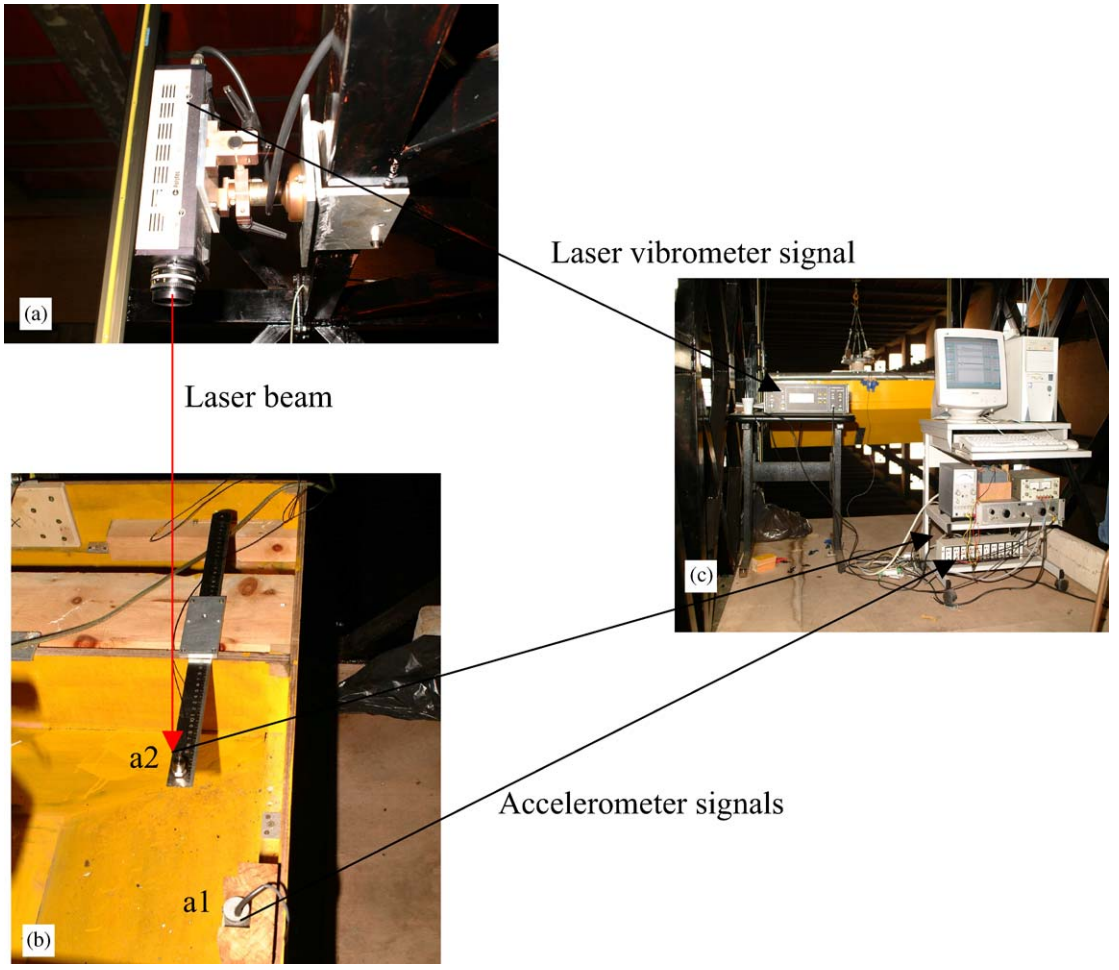

Fig. 8. Schematic of the experimental set up: (a) vibrometer laser head, at rest on the supporting frame—residual response measurements; (b) view of the on board measurement set up a1, accelerometer n.1, attached to the wedge structure—hydrodynamic force measurement—a2, accelerometer n.2, attached to beam's end—mounted only for overall response measurements; (c) conditioning and acquisition signal station.

the presence of the wire introduces a disturbance in the beam motion appearing essentially as a heavy increase of damping. Moreover this disturbance depends largely on the way the wire is fitted with respect to the beam (freely floating or attached to the beam itself). For these reasons a laser vibrometer has been preferred to realize a non-intrusive measure of the elastic residual response (see Fig. 8).

4. Experimental results

In the present section the results of the experimental tests are illustrated. More precisely, two different sets of measurements are performed. In Section 4.1 the analysis of the rigid-body motion of the wedge is considered focusing on the hydrodynamic force time history and its characteristic parameters F^* and t^*. On the other hand, the response of the elastic beam on board is investigated by a laser vibrometer technique. The analysis of both the residual and overall acceleration response is performed by comparing the results with those given in Section 2.2.

4.1. Rigid-body impact

A systematic series of tests was performed to measure the time history of the hydrodynamic force (special attention is addressed to F^* and t^*) and to compare the results with those given in Section 2.1.

The test height, varying between 0.25 and 2.00 m, is chosen in order to explore the velocity range between 1.5 and 5 m/s. The wedge is equipped with an accelerometer (see Table 1) that simply provides the hydrodynamic force accordingly with Eq. (1). To keep the actual value of the entry velocity, an integration of the free falling acceleration signal is performed.

The time history of the experimental acceleration signal is shown in Fig. 9(a) for the mass value $m = 46.8$ kg/m and impact velocities of 1.5, 3 and 5 m/s, respectively. The same measurements (Fig. 9(b)) have been performed with a wedge mass equal to 62.5 kg/m. The theoretical curves given in Section 2.1, correspond very satisfactorily with the experimental trend all along the impact stage, although some differences must be outlined and explained. For purpose of

Table 1
Experimental values of F^* and t^* for different entry velocities

Mass = 75 kg			
Height (m)	V_0 (m/s)	t^* (s)	F^* (N)
0.14	1.650	0.0302	1000.5
0.25	2.129	0.0253	1772
0.39	2.62	0.0206	2742.6
0.56	3.11	0.0158	3899
0.77	3.61	0.0124	5332.1
1.00	4.09	0.0122	6890.2
1.26	4.62	0.0111	8570.8
1.56	5.07	0.0085	10622.1

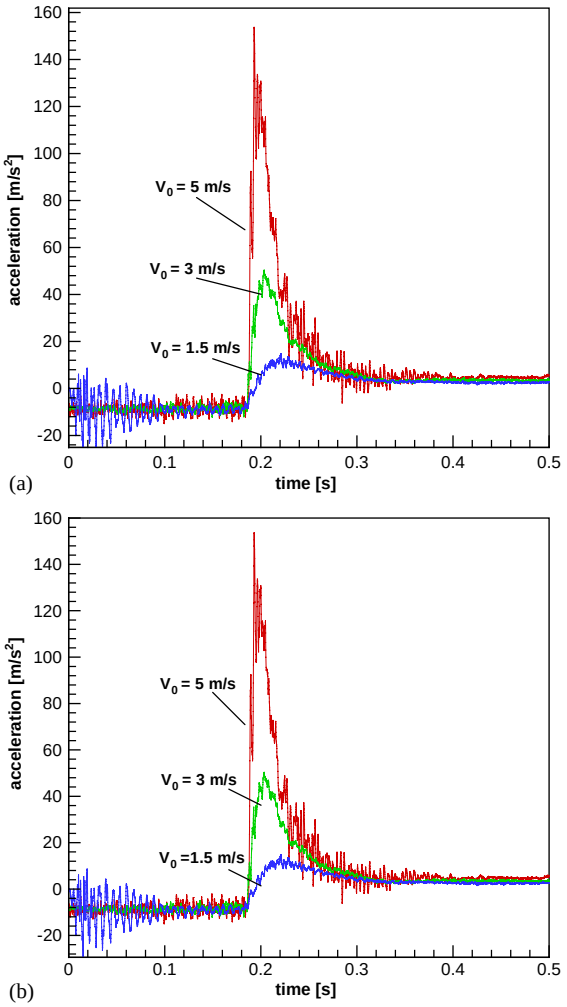

Fig. 9. Experimental time histories of the hydrodynamic forces for different entry velocities: (a) mass = 75 kg; (b) mass = 100 kg.

illustration in Fig. 10(a) and (b) the experimental time history of the hydrodynamic force is compared with the theoretical prediction given in Section 2.1.

Looking at the previous results, a first comment concerns the high-frequency disturbance superimposed on the rigid-body acceleration. In fact, the wedge does not behave as a perfect rigid body, as it is considered in the theoretical model, and responds with elastic vibrations when it is excited by the violent impact on the water, thus polluting the measurement signals. However, vibration noise is also observed in the first part of the signal before the water impact. This is in part due to the sudden removal of the wedge constraints thus exciting its vibration response. Moreover, during the free falling run, rail reactions, wheel-rail clearances and geometrical misalignments lead to excitation forces causing wedge vibrations. However, the frequency range of the mentioned disturbances is much higher than the frequency spectrum of the hydrodynamic

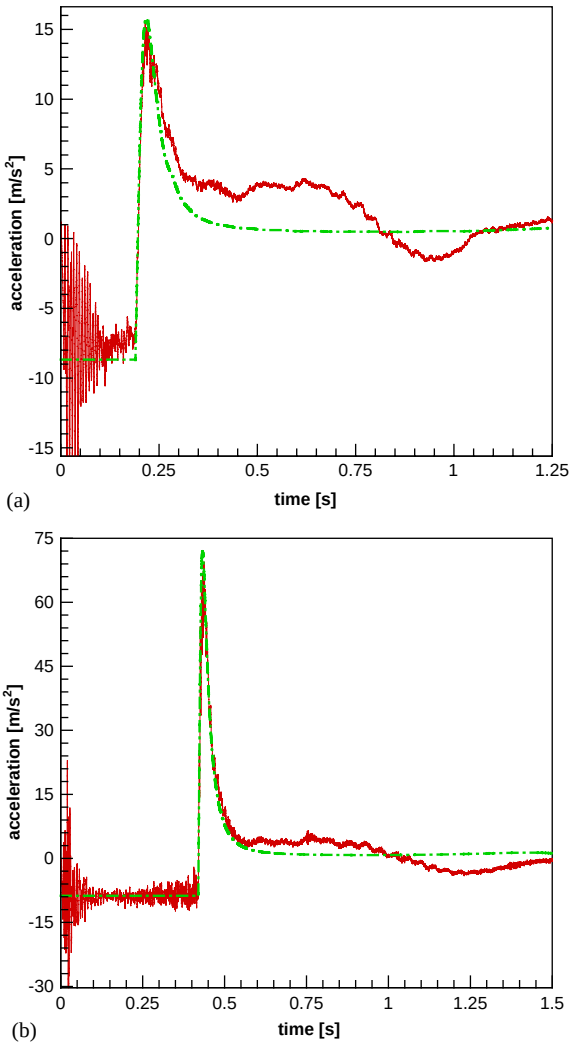

Fig. 10. Comparison between the theoretical and experimental results. (a) $V_0 = 1.5$ m/s, mass = 75 kg; (b) $V_0 = 3.5$ m/s, mass = 75 kg; — experimental; ·-·- theoretical.

force, allowing an effective separation between the rigid-body acceleration and that due to elastic vibrations.

Looking at the amplitude of the experimental maximum force, it is observed that it is always slightly lower than that expected by the theory. This fact is quite reasonable if the hypotheses of the theoretical model are kept in mind. In fact, although 3D effects have been reduced with the actual choice of the wedge sizes, as clarified in the previous section, they are not included in the theory so that some influence on the experimental measurements is expected because of the finite length of the wedge. Moreover, part of the energy given to the fluid is converted into propagating waves travelling along the water surface, while part is released to the water as a jet rising up along the wedge sides (Figs. 1 and 2) and, finally, part is elastically stored in the wedge and converted into elastic vibrations. All these effects are not modelled in Section 2.1.

Table 2
Experimental values of F^* and t^* for different entry velocities

Mass = 100 kg			
Height (m)	V_0 (m/s)	t^* (s)	F^* (N)
0.14	1.660	0.0428	1138.4
0.25	2.140	0.0290	2054.2
0.39	2.670	0.0223	3193.3
0.56	3.140	0.0207	4660.3
0.77	3.670	0.0159	6313.0
1.00	4.20	0.0153	8051.5
1.26	4.74	0.0126	10100
1.56	5.25	0.0099	12268.1

A final remark concerns the later part of the curves that is affected by a low-frequency disturbance; it is easily verified that this slow oscillation is due to the buoyancy force. This effect is more evident when the impact velocity is smaller (1.5 m/s) but it is negligible for the higher velocity (5 m/s) since, in this case, the hydrodynamic force is much higher with respect to the buoyancy force. In Tables 1 and 2, the experimental values of the entry velocity, the characteristic time t^* and the peak of the hydrodynamic force F^* are given for the cases mass = 75 and 100 kg, respectively. These values are obtained by filtering the vibration pollution in the force time history and averaging the results obtained over a repeated sequence of 10 tests for each height.

The dependency of F^* and t^* on v_0 and m can be investigated collecting the results of Tables 1 and 2 in Figs. 11(a) and (b). Both of them have the actual entry velocity on the x-axis, while on the vertical axis F^* and t^* are given in Figs. 11(a) and (b), respectively. In the same graphs the theoretical values of F^* and t^* are also represented. A good agreement between theory and experiments is found. However, some differences arise and, more precisely, the theoretical estimate of F^* is slightly higher than the experimental value, while the experimental t^* slightly exceeds the theoretical prediction. The previously mentioned arguments provide an explanation about the discrepancy for F^*. Moreover, since $F^*t^* \approx 0.247mv_0$ should be invariant (see Section 2.1), it is reasonably expected that when F^* is overestimated, then t^* is underestimated.

4.2. Overall and residual responses of the elastic system

As mentioned in Sections 2.2.2 and in 3, the elastic structure actually placed on board consists of a variable length aluminum beam. In Table 3 the measured values of the overall absolute acceleration spectrum, obtained by the experiments performed on the carried beam, are summarized providing the maximum measured peak of the acceleration (averaged over a set of five runs) and the first natural frequency of the beam (experimentally identified). In Fig. 12, the overall shock spectrum, determined on the basis of Table 3, is shown as a function of the first natural frequency of the beam. A harmonic modulation of the shock spectrum appears. This effect is simply explained by the following consideration. In the experimental tests the wedge experiences a free run before impacting the water. This means that the hydrodynamic force starts after a delay interval corresponding to the falling time $t_0 = \sqrt{2h_0/g}$, implying a time shift of the

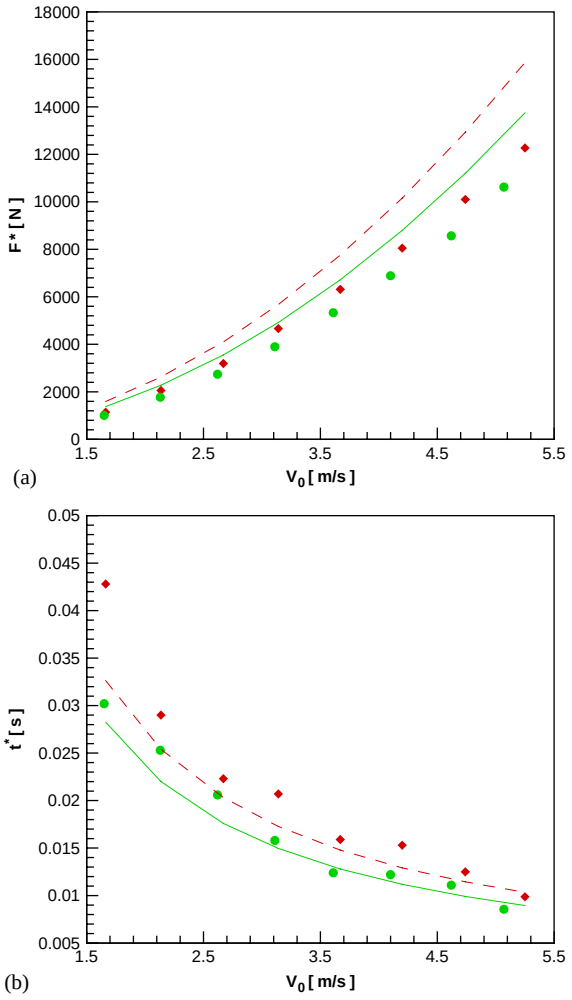

Fig. 11. (a) Comparison between the theoretical and experimental dependency of F^* on V_0; ▲ experimental mass = 75 kg; —— theoretical mass = 75 kg; ■ experimental mass = 100 kg; - - - theoretical mass = 100 kg. (b) Comparison between the theoretical and experimental dependency of t^* on V_0; ▲ experimental mass = 75 kg; —— theoretical mass = 75 kg; ■ experimental mass = 100 kg; - - - theoretical mass = 100 kg.

force waveform. This affects the shape of the shock spectrum, because the Fourier transform of the force presents a harmonic modulation with periodicity $2\pi/t_0$. This effect is simply introduced in the theoretical model (both for the overall and residual spectrum) by replacing $\tilde{F}_h(\tilde{t})$ with $\tilde{F}_h(\tilde{t}-\tilde{t}_0)$, where $\tilde{t}_0 = t_0/t^*$.

The maximum of the experimental overall spectrum is found at $f_n = 14$ Hz. In the same figure the comparison with the theoretical overall shock spectrum (Section 2.2) is given, showing a good agreement and an almost total superposition over the whole considered frequency range. The largest amplitude difference, 94.3 m/s^2 *vs* 80.5 m/s^2, corresponds to the relative maximum, but the critical corresponding frequencies are very close: 14 Hz for the experimental measurements

Table 3
Overall and residual acceleration functions of the first natural frequency of the beam

f_{n1}	$\bar{a}_{ov}$ (m/s^2)	f_{n1}	$\bar{a}_{ov}$ (m/s^2)
Overall acceleration			
3.50	53.33	24.55	68.82
4.88	55.33	26.80	64.18
6.71	68.05	28.39	70.28
8.25	56.86	28.86	69.30
9.45	78.64	31.30	62.26
11.00	71.80	31.74	68.00
11.85	64.05	34.50	61.56
12.82	86.69	35.69	58.65
14.0	94.27	39.41	55.65
15.25	64.87	41.00	47.39
17.10	77.61	43.65	53.16
17.70	83.00	47.29	47.88
19.65	64.52	56.32	45.13
20.60	73.35	73.51	43.40
$\tilde{f}_{n1sp}$	$\bar{a}_{res}$ (m/s^2)	$\tilde{f}_{n1sp}$	$\bar{a}_{res}$ (m/s^2)
Residual acceleration			
3.65	9.67	14.19	17.52
4.12	8.12	15.1	7.71
4.27	9.37	16.30	11.75
5.20	18.24	17.82	14.67
6.87	19	18.75	10.94
8.09	13.5	20.1	8.33
10.22	19.13	22.85	8.8
11.13	9.58	25.3	5.52
12.50	16.19	27.45	3.6

versus 13.3 Hz by using Eq. (31). These frequencies correspond to the dimensionless values 0.358 and 0.34, respectively, confirming the theoretical prediction of Section 2.2.2.

In Table 3 the measured values of the residual acceleration spectrum, following definition (24), are given together with the values of the corresponding natural frequency of the beam. The characteristic time appearing in Eq. (24) is $T \sim 50t^* \sim 1.25$ s, while the time interval is $\Delta T \sim 5$ s. In Fig. 13 the experimental curve corresponding to R given in Eq. (24) is plotted. Also in this case the frequency modulation due to the hydrodynamic time shift t_0 is apparent. In this case the comparison with the theoretical spectrum is not performed because, as has been explained in Section 2, the shape of the spectrum is affected by the dependency of the damping on frequency. As is well known, a procedure of damping identification is long and difficult, ultimately providing uncertain results. Thus, the analysis is addressed to validate the prediction of the critical frequency, i.e., the location of the maximum of the shock spectrum, rather than the evaluation of the actual amplitude.

The absolute maximum of the oscillating curve is found at 10.22 Hz, while the theoretical prediction provides, in absence of damping, 8.26 Hz corresponding to the dimensionless value 0.2.

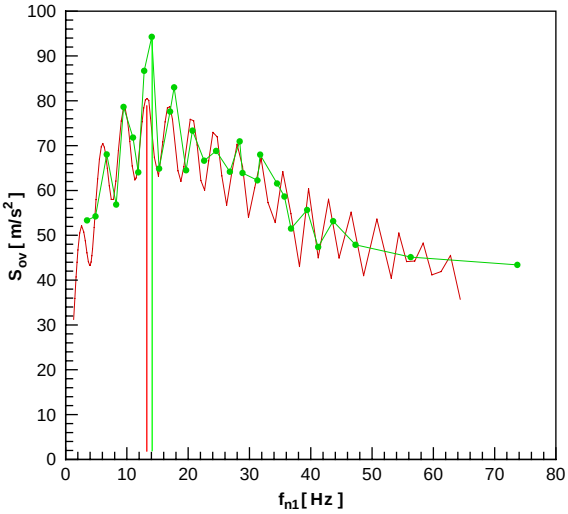

Fig. 12. Comparison between theoretical and experimental overall shock spectra; — theoretical; —□— experimental.

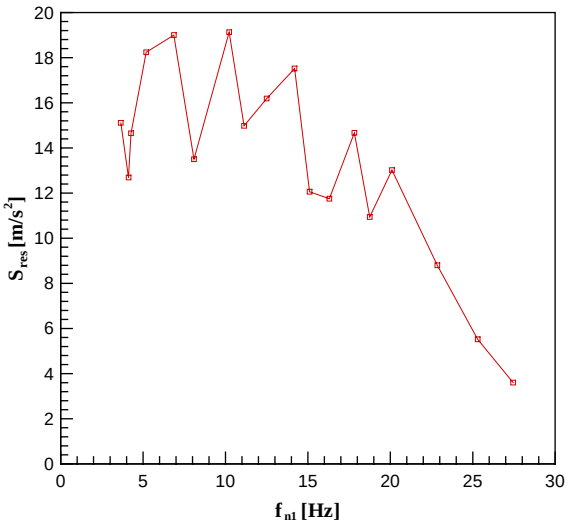

Fig. 13. Experimental residual shock spectrum.

However, looking at Fig. 12 and Table 3, it is apparent that the peak at 6.87 Hz is very close to the previous one, 19 m/s^2 *vs* 19.13 m/s^2, the difference ranging in the interval of the possible experimental errors. Moreover the frequency modulation effect may hide the exact location of the maximum. Thus, also looking at the trend exhibited in Fig. 12, the peak frequency of the spectrum can be reasonably estimated belonging to the interval 6.87–10.22 Hz. This is in good agreement with the value 8.26 Hz, provided by the theoretical prediction.

5. Conclusions

In this paper the impact of a freely falling wedge on the water surface is investigated. A first contribution of the paper centres around the development of a model taking into account the modification of the entry velocity of the wedge during the impact. In fact, the sudden deceleration of the wedge leads to a vanishing hydrodynamic force, after a sharp peak value at the early impact stage is reached. Two key parameters in the phenomenon have been identified: the rising time of the hydrodynamic force and the characteristic maximum of it. Their theoretical evaluation is provided by simple algebraic expressions in terms of the fundamental impact parameters, such as the wedge mass, the initial entry velocity and the deadrise angle. This dependency has been experimentally validated showing a fairly good agreement with the theoretical results.

The second contribution of the paper is concerned with the response of an elastic structure carried on-board the wedge. The impulsive behaviour of the hydrodynamic force is used to develop a model of the elastic response based on an effective tool such as the shock spectrum. By a suitable combination of the hydrodynamic model and the shock spectrum analysis, the chance of a simple a priori estimate of the worst suspension stiffness for a given mass on board is provided. Corresponding to this value, the oscillations of the carried mass due to the impact of the wedge lead to the most severe elastic force response.

The actual existence of such a "critical" phenomenon has been proven experimentally by a systematic set of tests performed on a clamped–free beam with variable length, mounted on the impacting wedge. The experimental results reveal that the maximum acceleration response of the beam occurs corresponding to a particular beam frequency (or length), very close to that predicted by the theoretical model.

Acknowledgements

The present work was supported by the Ministero delle Infrastrutture e dei Trasporti in the frame of INSEAN Research Program 2000-02.

References

[1] T. Von Karman, The impact of seaplane floats during landing, *National Advisory Committe for Aeronautics, Technical Memorandum* 321 (1929) 2–8.
[2] H. Wagner, Uber stoss gleitvergange an oberflache von flussigkeiten, *Zeitschrift für Angewandte Mathematik und Mechanik* 12 (1932) 192–215.
[3] W.H. Chu, H.N. Abramson, Hydrodynamic theories of ship slamming-review and extension, *Journal of Ship Research* (1961) 9–21.
[4] R.E.D. Bishop, W.G. Price, *Hydroelasticity of Ships*, Cambridge University Press, Cambridge, 1979.
[5] O. Belik, R.E.D. Bishop, W.G. Price, A simulation of ship responses due to slamming in irregular head sea, *RINA* 125 (1983) 237–253.
[6] J. Kvalsvold, O. Faltinsen, Hydroelastic modelling of wet deck slamming on multihull vessel, *Journal of Ship Research* 39 (3) (1995) 225–239.
[7] A. Korobkin, Wave impact on the bow end of a catamaran wet deck, *Journal of Ship Research* 39 (4) (1995) 321–327.

[8] A. Korobkin, Water impact problems in ship hydrodynamics, in: M. Ohkusu (Ed.), *Advances in Marine Hydrodynamics*, Kyushu University, Fukuoka, Japan, 1996, pp. 323–371.
[9] R. Zhao, O. Faltinsen, Water entry of arbitrary two-dimensional bodies, *Journal of Fluid Mechanics* 246 (1993) 593–612.
[10] W.S. Vorus, A flat cylinder theory for vessel impact and steady planing resistance, *Journal of Ship Research* 40 (2) (1996) 89–106.
[11] D. Battistin, A. Iafrati, Impact of 2D and axisymmetric bodies with arbitrary section on the water surface, in: *Proceedings of ECCOMAS 2001*, Swansea, UK, 2001.
[12] W.G. Price, P. Temarel, Water impact and hydroelasticity, in: *Proceedings of the International Seminar on Hydroelasticity for Ship Structural Design*, Genova, Italy, 1996.
[13] J. Kvalsvold, O. Faltinsen, Slamming loads on wetdecks of multihull vessels, in: O. Faltinsen (Ed.), *Hydroelasticity in Marine Technology*, Rotterdam, Balkema, 1994.
[14] D.J. Kim, W. Vorus, A. Troesh, R. Gollwitzer, Coupled hydrodynamic impact and elastic response, in: *Proceedings of 21st Symposium on Naval Hydrodynamics*, Trondheim, Norway, 1996, pp. 134–146.
[15] A. Carcaterra, E. Ciappi, A. Iafrati, E. Campana, Shock spectral analysis of elastic systems impacting on the water surface, *Journal of Sound and Vibration* 229 (3) (2000) 579–605.
[16] A. Iafrati, A. Carcaterra, E. Ciappi, E. Campana, Hydroelastic analysis of a simple oscillator impacting the free surface, *Journal of Ship Research* 44 (4) (2000) 278–289.
[17] W.S. Vorus, R.A. Royce, Wave impact reduction of planing boats, in: *Ship Structure Symposium 2000*, Arlington, Virginia, 2000.
[18] A. Carcaterra, F. La Gala, A shock spectral based control of slamming, in: *IX Congress of International Maritime Association of Mediterranean* (*IMAM 2000*), 2000, pp. 95–102.
[19] J.N. Newmann, *Marine Hydrodynamics*, MIT Press, Cambridge, MA, 1978.
[20] Z.N. Dobrovol' Skaya, On some problems of similarity flow of fluid with a free surface, *Journal of Fluid Mechanics* 36 (1969) 805–829.
[21] A. Carcaterra, E. Ciappi, Prediction of the compressible stage slamming force on rigid and elastic systems impacting on the water surface, *Nonlinear Dynamics* 21 (2000) 193–220.